Self-similar pseudobands and localization of magnetoplasmons in finite multilayered Fibonacci superlattices

Nian-hua Liu*
Pohl Institute of Solid State Physics, Tongji University, Shanghai 200092, People's Republic of China and Department of Physics, Ji An Teachers Training College, Ji An Jiangxi 343009, People's Republic of China

Wei-guo Feng†
Centre of Theoretical Physics, China Center for Advanced Science and Technology (World Laboratory), P.O. Box 8730, Beijing, People's Republic of China and Pohl Institute of Solid State Physics, Tongji University, Shanghai 200092, People's Republic of China

Xiang Wu‡
Centre of Theoretical Physics, China Center for Advanced Science and Technology (World Laboratory), P.O. Box 8730, Beijing, People's Republic of China; International Centre for Materials Physics, Academia Sinica, Shengyang, People's Republic of China; and Pohl Institute of Solid State Physics, Tongji University, Shanghai 200092, People's Republic of China
(Received 9 June 1993)

The collective plasmon-polariton excitations in finite Fibonacci semiconductor superlattices, which are subjected to a static magnetic field applied parallel to the interfaces, are studied by using local-field theory with retardation. We find that for a given in-plane wave vector, the discrete modes are composed of pseudobands and show rich self-similar patterns. The dispersion relations of the modes are obviously modified by the application of the magnetic field, and the propagation of the surface waves shows remarkable nonreciprocal behavior in the field. A number of coupled guided modes are found when the retardation effects are taken into account. We plot the profiles of the amplitudes to investigate the localization properties of the polaritons. The results show that those modes isolated from the pseudobands are localized, the modes located in the pseudobands are extended, while those located at the edges of the bands are critical.

I. INTRODUCTION

In recent years, much effort has been undertaken in the studies of the electronic and optical properties of superlattices. Because of the multilayered characteristic, knowledge about the interface excitations in the superlattices is of fundamental importance. It is known that the disturbances at individual interfaces coupled by the tails of the evanescent field can give rise to collective excitations of the whole system. The coupling of different layers depends critically upon the configuration of the superlattices. By changing the geometry of the structures, one can obtain various plasmon modes with different dispersion features.

The bulk plasmons of a periodic layered electron gas were extensively studied both theoretically[1–3] and experimentally.[4–6] The results show that the collective behavior in electron plasmas of the layered system is quite different from that either in a three-dimensional plasma or in a two-dimensional electron gas. A kind of surface polariton that can be supported by a semi-infinite layered electron gas, and which depends on the difference of the dielectric constants of the superlattice and the adjoining bulk insulator, was introduced in a previous theoretical work of Giuliani and Quinn[7] and was investigated experimentally by Dumelow *et al.* through measurements of attenuated total reflection spectroscopy.[8] For a periodic structure stacked by alternating dielectric slabs, Camley and Mills have given a systematic review on the collective excitations of the superlattices[9] and examined the dependence of the plasmons on the ratios of the thicknesses of alternating materials. The theoretical studies were extended by Constantinou and Cottam,[10] who included the effects of the charged sheets at the interfaces between the slabs and took the retardation into account. With the removal of the translational symmetry of the superlattices, as in a superlattice with a nonregular layer,[11] or a quasiperiodic region,[12] some new interface plasmon modes appear. The effects of an applied magnetic field on the plasmons are of great interest[13–15] because it changes the frequency of the collective excitations without changing the concentration of the carriers.

The quasiperiodic superlattices, which are generated with thicknesses mapping self-similar geometries, such as the Fibonacci sequence,[16] the Cantor sequence,[17] and so on, have attracted considerable attention in past years. As a result of the special geometries of the quasiperiodic systems, the electron energy spectra,[18–20] collective excitations,[21,22] and optical properties[23,24,17] reveal rich self-similar structures and scaling properties which are very different from those in the periodic systems. Recently, Johnson and Camley[25] and Albuquerque *et al.*[26,27] have investigated the magnetoplasmon of Fibonacci superlattices which are subjected to an external magnetic field ap-

plied parallel to the interfaces. They found that the number of the bands of the bulk modes for the quasiperiodic superlattice increases compared to the simple periodic system because the quasiperiodic unit cells become more complex. They also found the striking nonreciprocal propagations of the surface modes due to the application of the external field. However, they did not make further explorations on the properties resulting from the quasiperiodicity. For example, they did not examine the behavior of the modes when the generation becomes large and they did not discuss the important characteristic of self-similarity of the quasiperiodic system.

As an extension of the previous theoretical work, we investigate the magnetoplasmon-polariton excitations in this paper by considering a finite model of the Fibonacci superlattice and taking the retardation effects into account. In the finite case, the Bloch ansatz cannot be used, the dispersion equation is no longer of the form of $|\frac{1}{2}\mathrm{Tr}\underline{X}| \leq 1$ as that of infinite periodic structures, and the frequencies of the modes for a given in-plane wave vector consist of a discrete spectrum rather than a series of continuous bands.

The paper is organized as follows. In Sec. II we derive the dispersion relation of the magnetoplasmon modes by using local theory with retardation and the transfer-matrix method. Some numerical studies are presented in Sec. III, where we show the pseudoband structure of the discrete modes with self-similar patterns, we investigate the effects of an applied magnetic field and retardation on the dispersion relations, and we discuss the localization properties of the polaritons. In Sec. IV we give a brief summary of the numerical results.

II. THEORY

The system under consideration, which was regarded as a unit cell of an infinite array in Ref. 25, is composed of two alternating blocks L and S along the z axis and following the rule of Fibonacci sequence, that is, $\{C_n\}=\{C_{n-1}C_{n-2}\}$ with $\{C_0\}=\{S\}$ and $\{C_1\}=\{L\}$. Each block contains two different materials A and B with thicknesses d_{AL}, d_{BL} for block L and d_{AS}, d_{BS} for block S, respectively. We neglect the quantization effects as in Ref. 25, and assume that the properties of the slabs can be described by macroscopic dielectric functions. The external magnetic field is taken to be parallel to the y axis, thus the dielectric tensor for a given layer can be expressed as

$$\epsilon_\mu=\begin{bmatrix} \epsilon_{1\mu} & 0 & -i\epsilon_{2\mu} \\ 0 & \epsilon_{3\mu} & 0 \\ i\epsilon_{2\mu} & 0 & \epsilon_{1\mu} \end{bmatrix}, \tag{1}$$

where

$$\epsilon_{1\mu}=\epsilon_{\infty\mu}[1+\omega_{P\mu}^2/(\omega_c^2-\omega^2)] , \tag{2}$$

$$\epsilon_{2\mu}=\epsilon_{\infty\mu}\omega_{P\mu}^2\omega_c/\omega(\omega_c^2-\omega^2) , \tag{3}$$

$$\epsilon_{3\mu}=\epsilon_{\infty\mu}(1-\omega_{P\mu}^2/\omega^2) , \quad \mu=A,B , \tag{4}$$

with ω_c denoting the cyclotron frequency, $\omega_{P\mu}$ the plasma frequency of the relevant material, and the subscript ∞ referring to the background dielectric constant.

We consider p-polarized modes propagating in the direction of the x axis with wave vector q. The electric and magnetic fields of the modes are written as

$$\mathbf{E}=(E_x,0,E_z), \quad \mathbf{H}=(0,H_y,0) . \tag{5}$$

After solving Maxwell equations for a general layer, we find that the electric and magnetic fields at any two positions in the layer satisfy the following matrix equation:

$$\begin{bmatrix}\phi\\ \psi\end{bmatrix}_{z+\Delta z}=\underline{M}_\mu(\Delta z)\begin{bmatrix}\phi\\ \psi\end{bmatrix}_z , \tag{6}$$

where the functions ϕ and ψ are related to the tangential components of the electric and magnetic fields and are defined as

$$\phi\equiv E_x , \quad \psi\equiv -i\mu_0 cH_y , \tag{7}$$

and the elements of matrix $\underline{M}_\mu(\Delta z)$ are given by

$$m_{11}=\cosh\alpha_\mu\Delta z+\frac{q\epsilon_{2\mu}}{\alpha_\mu\epsilon_{1\mu}}\sinh\alpha_\mu\Delta z , \tag{8}$$

$$m_{12}=\frac{\alpha_\mu\omega}{c(q^2-\alpha_\mu^2)}\left[1-\left[\frac{q\epsilon_{2\mu}}{\alpha_\mu\epsilon_{1\mu}}\right]^2\right]\sinh\alpha_\mu\Delta z , \tag{9}$$

$$m_{21}=\frac{c(q^2-\alpha_\mu^2)}{\alpha_\mu\omega}\sinh\alpha_\mu\Delta z , \tag{10}$$

$$m_{22}=\cosh\alpha_\mu\Delta z-\frac{q\epsilon_{2\mu}}{\alpha_\mu\epsilon_{1\mu}}\sinh\alpha_\mu\Delta z , \tag{11}$$

$$\mu=A,B ,$$

where

$$\alpha_\mu=\begin{cases} [q^2-\frac{\omega^2}{c^2}\epsilon_{V\mu}]^{1/2} & \text{if } q^2-\frac{\omega^2}{c^2}\epsilon_{V\mu}>0 \\ -i\left[\frac{\omega^2}{c^2}\epsilon_{V\mu}-q^2\right]^{1/2} & \text{if } q^2-\frac{\omega^2}{c^2}\epsilon_{V\mu}<0 \end{cases} \tag{12}$$

and $\epsilon_{V\mu}=(\epsilon_{1\mu}^2-\epsilon_{2\mu}^2)/(\epsilon_{1\mu})$ is the so-called Voigt dielectric function.

If we omit the presence of charged carriers at the interfaces, as in Ref. 25, then the tangential components of the electric and magnetic fields are continuous across the interfaces according to the standard boundary conditions of the electromagnetic field. The continuity of the fields enables us to connect any two positions of the fields in the superlattice by a product of matrices. Obviously, the electric and magnetic fields can be connected by the following transfer-matrix relation:

$$\begin{bmatrix}\phi\\ \psi\end{bmatrix}_{z=d_n}=\underline{X}_N\begin{bmatrix}\phi\\ \psi\end{bmatrix}_{z=0} , \tag{13}$$

where

$$d_n = F_{n-1}(d_{AL}+d_{BL})+F_{n-2}(d_{AS}+d_{BS}) \tag{14}$$

is the total thickness of the superlattice,

$$\underline{X}_N = \prod_{j=1}^{N} \underline{M}_\mu(d_j) \tag{15}$$

is the product of matrices with the order mapping the thicknesses of the superlattice, and the nth Fibonacci number is defined as $F_n = F_{n-1}+F_{n-2}$ with $F_1 = F_0 = 1$, while $N = 2F_n$ is the total number of the layers.

We assume that the superlattice rests on a substrate of dielectric ϵ_N and is adjoined by a vacuum at the top. After taking the solutions which fall to zero exponentially as one moves away from the surfaces at the top and the bottom, and matching the boundary conditions across the two surfaces, we obtain the dispersion relation of the modes as

$$\zeta_N x_{11}+\zeta_0 x_{22}-\zeta_N\zeta_0 x_{12}-x_{21}=0 , \tag{16}$$

where x_{ij} is the element of the matrix $\underline{X}_N$ and

$$\zeta_\nu = \frac{c}{\omega}\alpha_\nu(1-q^2/\alpha_\nu^2) . \tag{17}$$

Here

$$\alpha_\nu = \left[q^2-\frac{\omega^2}{c^2}\epsilon_\nu\right] , \quad \nu = N,0 \tag{18}$$

and the subscripts N and 0 correspond to the substrate and vacuum, respectively.

III. NUMERICAL EXAMPLES

In this section, we present some numerical studies of the dispersion relation and the localization properties of the plasmon-polariton modes for the finite Fibonacci superlattices. Following Johnson *et al.*,[13,25,28] we choose the model system as a GaAs superlattice in which only A layers are doped with the plasma frequency $\omega_{PA} = 0.04075$ eV and the material B and substrate are both undoped GaAs. The background dielectric constants are taken as $\epsilon_{\infty A} = \epsilon_{\infty B} = \epsilon_N = 13.13$. For simplicity, we introduce dimensionless quantities $\Omega = \omega/\omega_{PA}$, $Q = qc/\omega_{PA}$, and $D_j = d_j\omega_{PA}/c$. The dimensionless thickness D_{AL} is chosen as 0.1, which means $d_{AL} = 484$ nm, and the other parameters are $D_{BL} = 0.5D_{AL}$, $D_{BS} = 0.5D_{AS}$, and $(D_{AL}+D_{BL})/(D_{AS}+D_{BS}) = (\sqrt{5}+1)/2$ (golden mean). All of these ratios are the same as in Ref. 25.

A. Without the applied magnetic field

Let us first examine the case without the external magnetic field. In Fig. 1, we show the dispersion curves of the plasmon-polariton modes for the fourth generation Fibonacci superlattice. The dashed line in the figure represents the light line of $\omega = qc/\sqrt{\epsilon_N}$. As we have seen from the figure, there are ten dispersion curves corresponding respectively to five acousticlike and five opticlike branches. The highest acousticlike modes rise from the original with a slope almost identical to the light line

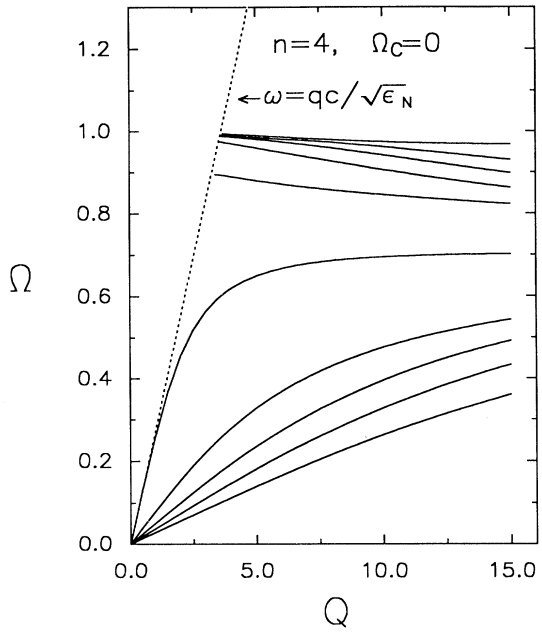

FIG. 1. Dispersion curves for the fourth Fibonacci superlattice in the case without an applied magnetic field.

and approach the asymptotic limit of the surface plasma frequency $\omega_{SA} \equiv \omega_{PA}/\sqrt{2}$ at a large wave vector. The polaritons in this branch behavior very similarly to photons at a small wave vector but like surface plasmons at the other limit. In Fig. 2, we have plotted the amplitudes of electric field E_x for two modes in this branch with different wave vectors $Q = 1$ and $Q = 10$. The modes, as shown in the figure, are mainly located at the bottom (note that the last interface, in fact, means nothing since we assume that the materials of the substrate and B layers are both undoped GaAs), but the one with a larger

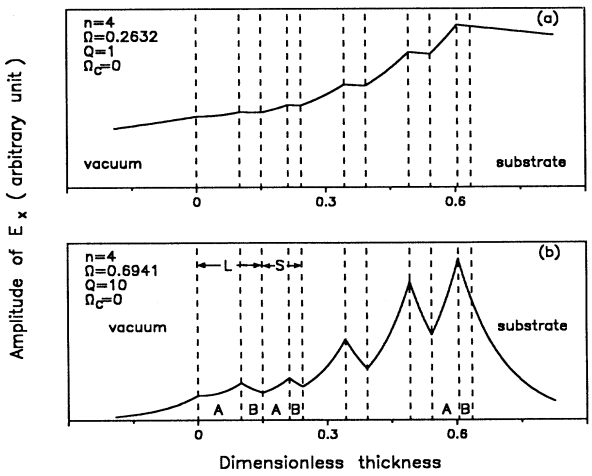

FIG. 2. Amplitudes of the electric field for two acousticlike surface modes with a different wave vector. The relevant parameters are shown in the figure.

wave vector has obvious interface characteristics compared to the other. The amplitudes of the next four acousticlike modes are shown in Fig. 3. One can see the different localization features of the polaritons for different branches.

With increasing the generation of the Fibonacci sequence, the polariton modes become more and more rich. Generally, the number of the branches, both acousticlike and opticlike, is equal to F_n, the total number of blocks in the Fibonacci superlattice. For a given wave vector $Q=10$, we show in Fig. 4 the discrete frequencies vs the generation number n. One can clearly see that when n becomes large, the discrete modes form a series of quasicontinuous bands and only a few isolated modes appear in the gaps. The pseudobands have distinct edges which are not variable with n. By plotting the amplitudes, as shown in Fig. 5, we find that the isolated modes located in the gaps are localized surface states [see Fig. 5(a)] and those located in the middle of the bands are extended states [see Fig. 5(b)]. Those located at the edges of the bands become critical [see Fig. 5(c)]; they are neither extended states nor localized states. In the larger gap around $\Omega=0.3$, as shown in Fig. 4, there are some modes which exist only if n is even, and the similar modes occur also in the high frequency region. In fact, whether these modes appear or not depends on the configuration of the superlattice; they appear only if the last block is S.

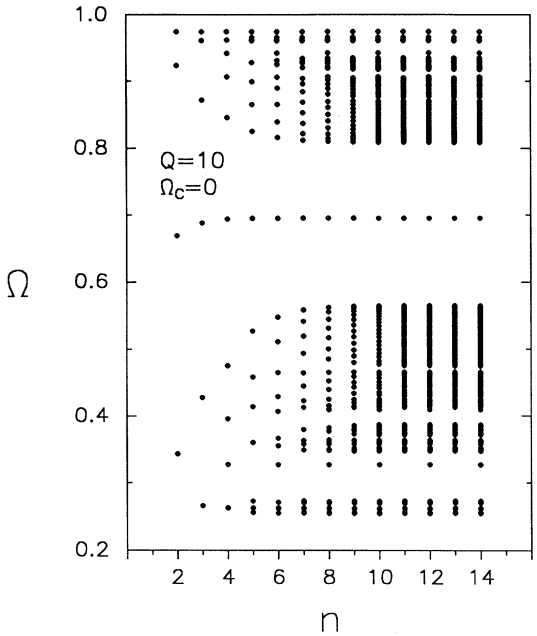

FIG. 4. Pseudobands of polaritons for the given wave vector $Q=10$ in the case without an applied magnetic field.

In Fig. 6, we show the density of modes for $n=12$ (note the logarithmic scale for the density of the modes). It is found that the distribution of the modes in the bands near the surface frequency ω_{SA} is uniform relatively, but

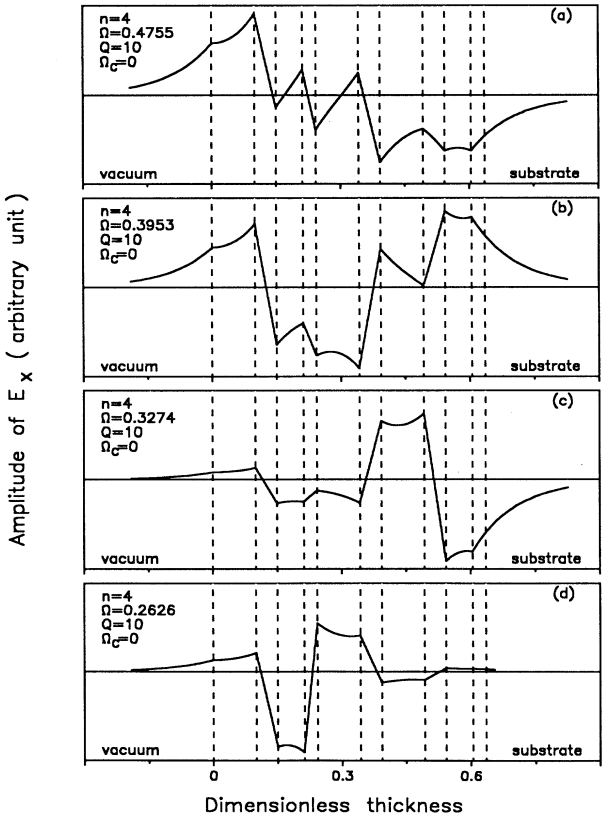

FIG. 3. Amplitudes of the electric field for four acousticlike interface modes with the same wave vector but with different frequencies. The relevant parameters are shown in the figure.

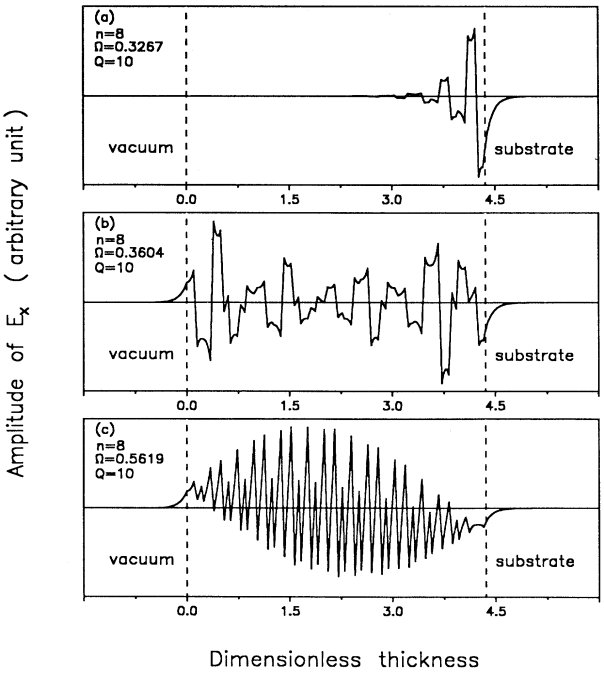

FIG. 5. Three typical amplitudes of polaritons for the eighth Fibonacci superlattice in the case without an applied magnetic field: (a) the localized state, (b) the extended state, and (c) the critical state. The relevant parameters are shown in the figure.

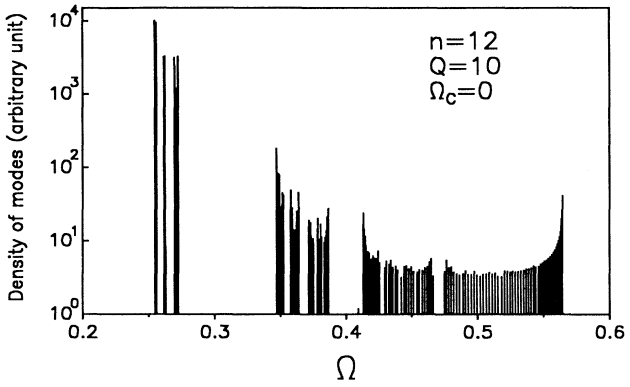

FIG. 6. Density of modes of the 12th Fibonacci superlattice for the given wave vector $Q=10$. Note the logarithmic scale for the density of modes.

in the other bands the density fluctuate rapidly. In fact, this fluctuation originates from the self-similar structure of the frequency spectrum. Due to the self-similar construction of the system, the frequency of the polaritons presents well defined self-similar patterns. In Fig. 7, we show two typical pictures of the self-similar modes. The upper plan corresponds to the generation numbers $n=5-12$ with the frequency interval of $\Omega=0.344-0.390$. The region closed by the dashed line in plan (a) is enlarged in the lower plan (b), which corresponds to $n=7-14$ with $\Omega=0.3466-0.3530$. One can clearly see the invariability with changing the scale of the frequency.

B. In the external magnetic field

Now we turn to consider the effects of the applied magnetic field on the polaritons. It is known that the striking

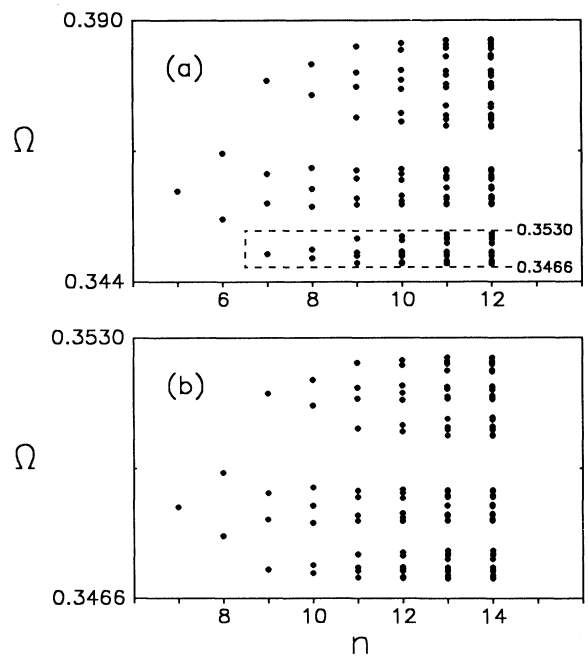

FIG. 7. Self-similar patterns of the pseudobands of polaritons. The relevant parameters are the same as in Fig. 4.

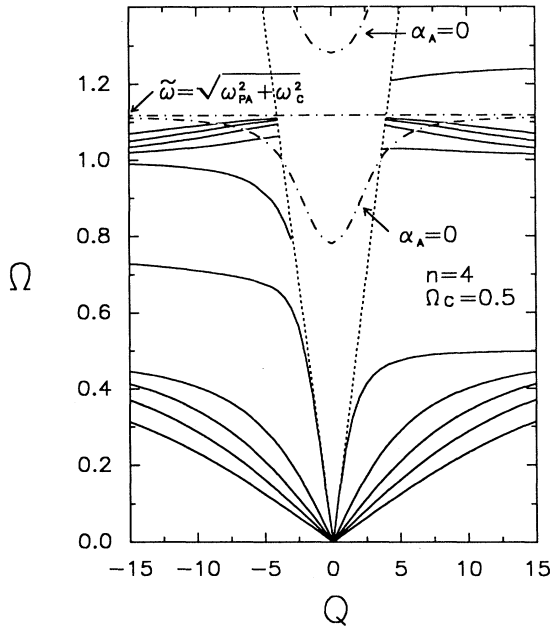

FIG. 8. Dispersion curves for the fourth Fibonacci superlattice, which is subjected to an applied magnetic field with the cyclotron frequency $\Omega_C=0.5$. The region between the straight dash-dotted line of $\tilde{\omega}=\sqrt{\omega_{PA}^2+\omega_C^2}$ and the lower dash-dotted line of $\alpha_A=0$ corresponds to coupled guided modes.

result caused by the application of the external field is the nonreciprocal propagation of the surface modes. The nonreciprocal propagation, as indicated in Ref. 25, could be important for device applications.

In Fig. 8, we show the dispersion curves also for the fourth Fibonacci superlattice, but it is now put in an external magnetic field with the cyclotron frequency $\Omega_C=0.5$. Obviously, the dispersion relations are modified by the applied field, as shown in the figure. On the positive wave vector side, all of the modes remove towards higher and lower frequencies due to the application of the field. As we reverse the propagation direction, that is, let $Q\rightarrow -Q$, the dispersion curves for the corresponding surface modes become quite different. In Fig. 9, we plot the curves of frequency vs the cyclotron frequency to show the dependence of the polariton on the applied magnetic field. The real lines and open circle lines in the figure represent the modes with negative and positive wave vectors, respectively. As shown in the figure, the two kind of modes with opposite propagation directions in the field have very different behaviors: the one with positive Q increases or decreases monotonically, but the other with negative Q has two branches of surface modes in the middle which tend to move closer to each other at first, but separate in the situation of strong magnetic field. Only the frequencies of the surface modes are altered apparently by reversing the propagation direction. As we have seen from Fig. 9, the frequencies of the other interface modes are almost invariable with changing Q for $-Q$.

For the surface modes, not only the frequencies are

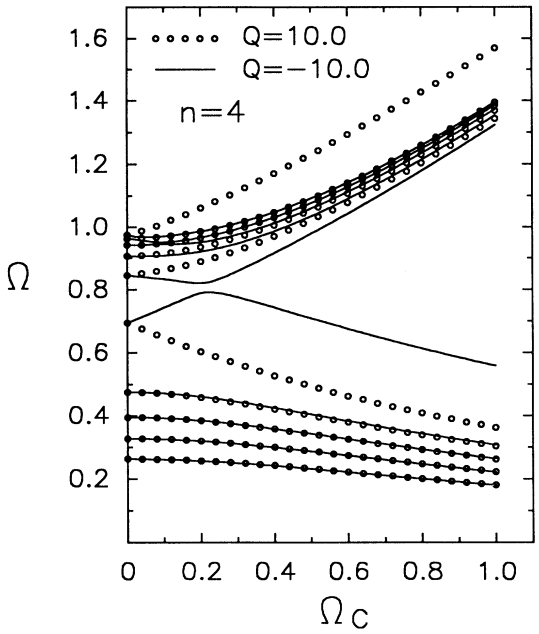

FIG. 9. Frequency of the magnetoplasmon polaritons in the opposite propagation directions vs the cyclotron frequency. The solid lines are for the modes with a negative wave vector and the lines with open circles are for the modes with a positive wave vector.

shifted when we reverse the propagation direction, but also the localization features are changed. In Fig. 10, we plot the amplitudes of the uppermost acousticlike surface modes with opposite wave vector. It is found that the localization features of the modes are quite different: the one with $Q=10$ is localized at the bottom and the other with $Q=-10$ at the top. Although the frequencies of the other interface modes are not so obviously altered by reversing the propagation direction as that of the surface

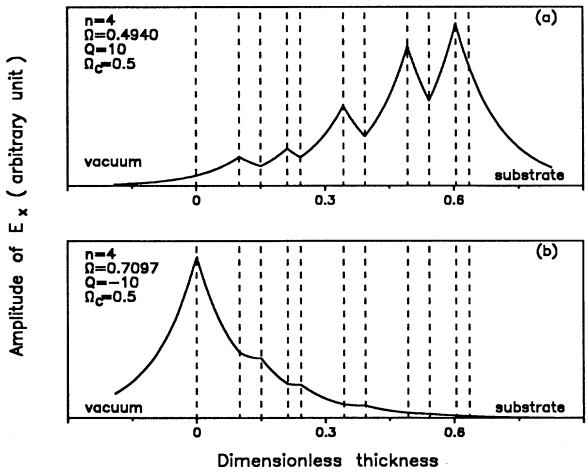

FIG. 10. Amplitudes of the electric field for two acousticlike surface modes in the applied magnetic field with opposite wave vector. The relevant parameters are shown in the figure.

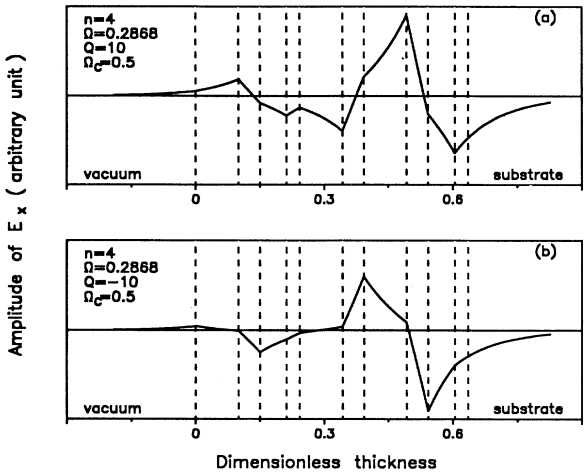

FIG. 11. Amplitudes of the electric field for two acousticlike interface modes in the applied magnetic field with opposite wave vector. The relevant parameters are shown in the figure.

modes, the localization features of the modes are not the same, as shown in Fig. 11, where the two amplitudes correspond to a pair of modes with the same frequency but with opposite wave vector. From the figure one can see that the two corresponding modes are located at different interfaces. Comparing Fig. 11(a) with Fig. 3(c), the amplitudes in the figures stand for two corresponding modes in the second acousticlike branch in the cases with and without the applied magnetic field. We find that the polariton is more strongly localized at the interfaces by the applied field.

Now we return to examine Fig. 8. The dash-dotted lines in the figure divide the Ω-Q plane into the regions of interface modes and guided modes according to whether the decay factor α_A is real or imaginary. In the region between the straight dashed-dotted line of $\tilde{\omega}=\sqrt{\omega_{PA}^2+\omega_C^2}$ and the lower dash-dotted line of $\alpha_A=0$, the polaritons are propagating instead of the evanescent field in the A layers because α_A is an imaginary number, that is, the collective excitations are cou-

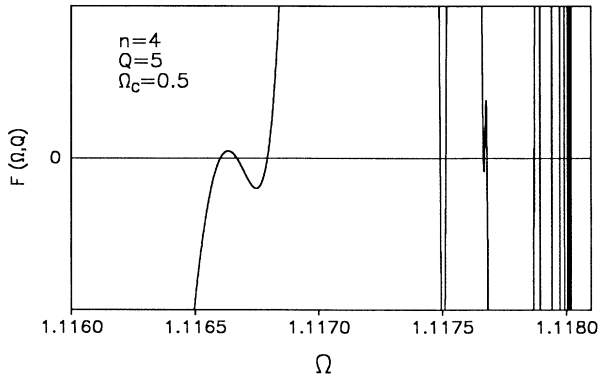

FIG. 12. The function defined by Eq. (19) vs frequency. The zero points of the function correspond to the solutions of the coupled guided modes.

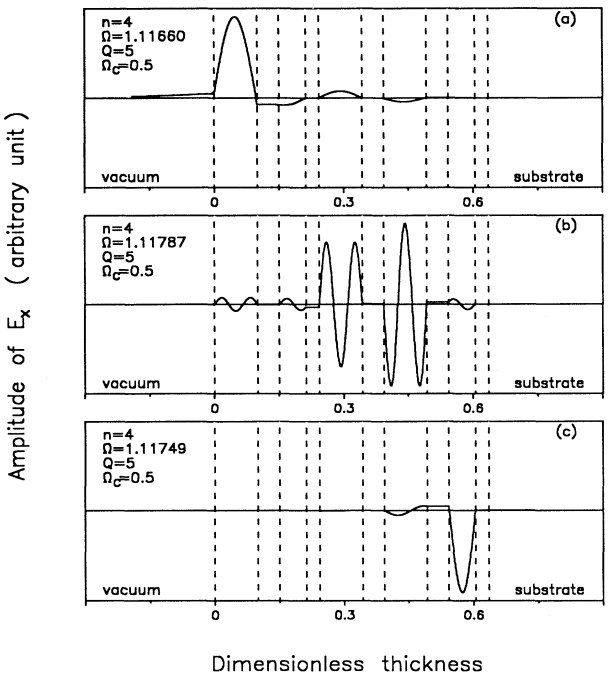

FIG. 13. Amplitudes of the electric field for three coupled guided modes with the same wave vector but with different frequencies. The relevant parameters are shown in the figure.

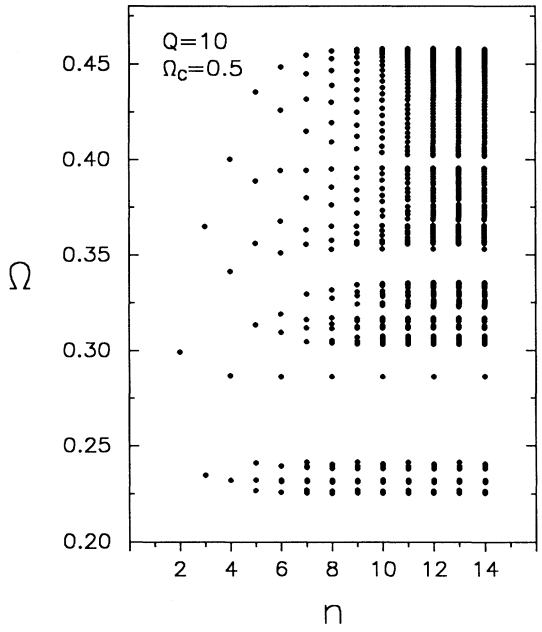

FIG. 14. Self-similar patterns of the pseudobands of polaritons in the applied magnetic field with the cyclotron frequency $\Omega_C=0.5$ and the given wave vector $Q=10$.

pled guided modes. At the frequency $\tilde{\omega}$, the dielectric $\epsilon_{1A}=0$ and α_A becomes singular. When the frequency approaches $\tilde{\omega}$ from the lower side, the function defined by the left-side of the dispersion equation (16), that is,

$$f(\omega,q)=\zeta_N x_{11}+\zeta_0 x_{22}-\zeta_N\zeta_0 x_{12}-x_{21}\ , \tag{19}$$

rises and falls rapidly though the frequency axis, as shown in Fig. 12, which gives a number of solutions for the coupled guided modes. These modes are not shown in Fig. 8 because they are too close to the dash-dotted line of $\tilde{\omega}$ to be resolved. Three amplitudes of these modes are shown in Fig. 13. From the figure we can see that the guided modes are coupled by the tails of the evanescent field out of the active layers and have different localization behaviors though the differences in frequency are very small. It should be indicated that this case is omitted in the nonretardation approximation.

Finally, we show the pseudobands of the polaritons in the external magnetic field in Fig. 14, with the range of frequency corresponding to the acousticlike modes except for the surface modes that are far from the bands. As shown in the figure, the applied field shifts the frequencies, but does not change the self-similar structure. The reason is that the self-similarity of the frequency spectrum is the characteristic of geometry of the quasiperiodic system, which cannot be changed by the external field.

IV. SUMMARY

We have extended the theoretical work on the collective magnetoplasmon polariton excitations to the case of finite quasiperiodic Fibonacci superlattices. The dispersion relations and the localization properties of the modes are investigated by using numerical examples. It is found that the polariton modes are composed of pseudobands with rich self-similar structures and the self-similarity is not destroyed by the external magnetic field. The applied magnetic field obviously modifies the dispersion relations and localization features of the polaritons and gives rise to the remarkable nonreciprocal propagations of the surface waves. Because the effects of retardation are taken into account, we found a number of coupled guided modes. The plasmon-polariton excitations, as we know, can be observed experimentally by, for example, inelastic light scattering,[4–6] far infrared attenuated total reflection spectroscopy,[8] or electron-energy-loss spectroscopy.[29] We hope that our theoretical results stimulate the interest of exprimentalists.

ACKNOWLEDGMENTS

We gratefully acknowledge useful conversations with Professor Yu-mei Zhang and Professor Hong Chen. Part of this work was supported by the Chinese National Advanced Technology Foundation through Grant No. 040-144-05-085.

*Permanent address: Department of Physics, Ji An Teachers Training College, Ji An, Jiangxi 343009, People's Republic of China.

†Permanent address: Pohl Institute of Solid State Physics, Tongji University, Shanghai 200092, People's Republic of China.

‡Permanent address: Pohl Institute of Solid State Physics, Tongji University, Shanghai 200092, People's Republic of China.

[1]A. L. Fetter, Ann. Phys. (N.Y.) **88**, 1 (1974).

[2]S. Das Sarma and J. J. Quinn, Phys. Rev. B **25**, 7603 (1982).

[3]J. K. Jain and P. B. Allen, Phys. Rev. Lett. **54**, 947 (1985); Phys. Rev. B **32**, 997 (1985).

[4]D. Olego, A. Pinczuk, A. C. Gossard, and W. Wiegmann, Phys. Rev. B **25**, 7867 (1982).

[5]A. Pinczuk, M. G. Lamont, and A. C. Gossard, Phys. Rev. Lett. **56**, 2092 (1986).

[6]G. Fasol, N. Mestres, H. P. Hughes, A. Fischer, and K. Ploog, Phys. Rev. Lett. **56**, 2517 (1986).

[7]G. F. Giuliani and J. J. Quinn, Phys. Rev. Lett. **51**, 919 (1983).

[8]T. Dumelow, T. J. Parker, D. R. Tilley, R. B. Beall, and J. J. Harris, Solid State Commun. **77**, 253 (1991).

[9]R. E. Camley and D. L. Mills, Phys. Rev. B **29**, 1695 (1984).

[10]N. C. Constantinou and Cottam, J. Phys. C **19**, 739 (1986).

[11]W. L. Bloss, J. Appl. Phys. **69**, 3068 (1991); Phys. Rev. B **44**, 1105 (1991).

[12]N. H. Liu, W. G. Feng, and X. Wu, J. Phys. Condens. Matter **4**, 9823 (1992).

[13]B. L. Johnson and R. E. Camley, Phys. Rev. B **38**, 3311 (1988).

[14]E. L. Albuquerque, P. Fulco, G. A. Farias, M. M. Auto, and D. R. Tilley, Phys. Rev. B **43**, 2032 (1991).

[15]Manvir S. Kushwaha, Phys. Rev. B **40**, 1692 (1989); **41**, 5602 (1990).

[16]R. Merlin, K. Bajema, R. Clarke, F. Y. Juang, and P. K. Bhattacharya, Phys. Rev. Lett. **55**, 1768 (1985); J. Todd, R. Merlin, R. Clarke, K. M. Mohanty, and J. D. Axe, *ibid.* **57**, 1157 (1986).

[17]X. Wu, H. S. Yao, and W. G. Feng, Proc. SPIE **1519**, 625 (1991); W. G. Feng, N. H. Liu, and X. Wu, *ibid.* Proc. SPIE **1928**, 286 (1993); N. H. Liu, W. G. Feng, and X. Wu, J. Phys. Condens. Matter **5**, 4623 (1993).

[18]S.-R. Eric Yang and S. Das. Sarma, Phys. Rev. B **37**, 4007 (1988).

[19]Y. Y. Wang and J. C. Maan, Phys. Rev. B **40**, 1955 (1989).

[20]D. Toet, M. Potemski, Y. Y. Wang, and J. C. Maan, Phys. Rev. Lett. **66**, 2128 (1988).

[21]P. Hawrylak and J. J. Quinn, Phys. Rev. Lett. **57**, 380 (1986); P. Hawrylak, G. Eliasson, and J. J. Quinn, Phys. Rev. B **36**, 6501 (1987).

[22]D. H. Huang, J. P. Peng, and S. X. Zhou, Phys. Rev. B **40**, 7754 (1989).

[23]W. G. Feng, N. H. Liu, and X. Wu, Phys. Rev. B **43**, 6893 (1991).

[24]W. G. Feng, W. Z. He, D. P. Xue, Y. B. Xu, and X. Wu, J. Phys.: Condens. Matter **1**, 8241 (1989).

[25]B. L. Johnson and R. E. Camley, Phys. Rev. B **44**, 1225 (1991).

[26]E. L. Albuquerque and Cottam, Solid State Commun. **81**, 383 (1992).

[27]G. A. Farias, M. M. Auto, and E. L. Albuquerque, Phys. Rev. B **38**, 12 540 (1988).

[28]B. L. Johnson, J. T. Weiler, and R. E. Camley, Phys. Rev. B **32**, 6544 (1985).

[29]M. Rocca, M. Lazzarino, and U. Valbusa, Phys. Rev. Lett. **69**, 2122 (1992).